

# Fragmentation of Massive Protostellar Disks

Kaitlin M. Kratter<sup>a</sup> and Christopher D. Matzner<sup>a</sup>

<sup>a</sup>*Department of Astronomy & Astrophysics*

*University of Toronto, 50 St. George Street, Toronto, ON M5S 3H4, Canada*

printed 21 June 2018

## ABSTRACT

We examine whether massive-star accretion disks are likely to fragment due to self-gravity. Rapid accretion and high angular momentum push these disks toward fragmentation, whereas viscous heating and the high protostellar luminosity stabilize them. We find that for a broad range of protostar masses and for reasonable accretion times, massive disks larger than  $\sim 150$  AU are prone to fragmentation. We develop an analytical estimate for the angular momentum of accreted material, extending the analysis of Matzner and Levin to account for strongly turbulent initial conditions. In a core-collapse model, we predict that disks are marginally prone to fragmentation around stars of about four to  $15 M_{\odot}$  – even if we adopt conservative estimates of the disks’ radii and tendency to fragment. More massive stars are progressively more likely to fragment, and there is a sharp drop in the stability of disk accretion at the very high accretion rates expected above 110 solar masses. Fragmentation may starve accretion in massive stars, especially above this limit, and is likely to create swarms of small, coplanar companions.

## 1 INTRODUCTION

Advances in submillimeter telescope have enabled the discovery of flattened structures, in some cases clearly Keplerian disks, surrounding massive ( $\gtrsim 10M_{\odot}$ ) protostars (Cesaroni 2005; Chini et al. 2004; Patel et al. 2005; Beuther et al. 2006). The logical inference – that high mass star formation (HMSF) proceeds through disk accretion – raises a question: can such disks process rapid mass accretion, or do they fragment to produce secondary stars? We seek to answer this question by estimating the criterion for disk fragmentation in the vicinity of a massive star.

If massive-star disks typically do not fragment, then disk accretion poses little barrier to massive star formation. Conversely if disk fragmentation occurs, then accretion onto the central star may be (partially) choked off, as suggested by Tan & Blackman (2005) in the context of low-luminosity active galactic nuclei. Moreover each massive star that forms from a fragmenting disk may be surrounded by smaller stars that began as disk fragments. It is therefore important to evaluate models for HMSF in light of the disk fragmentation criterion.

The current work uses and extends the results of Matzner & Levin (2005, hereafter ML05), who showed that protostellar disks around low mass stars are strongly stabilized against fragmentation by a combination of viscous heating and irradiation by the central protostar. Massive star formation is fundamentally different, however, in three important ways. The rapid rise of luminosity with mass implies that stellar irradiation is far more intense; this tends to stabilize disks against fragmentation. However, massive stars must accrete quickly to form at all (e.g., Wolfire & Cassinelli

1987), and rapid accretion favors fragmentation. These effects compete to set the critical radius outside of which disks fragment. Whether fragmentation actually occurs depends on the initial disk radius, which itself depends on the physical state of the gas prior to accretion. We discuss disk fragmentation in §2, considering the stabilizing effect of viscous heating (§2.2) before incorporating irradiation by the central star (§2.3). This combination allows us to identify (§2.4) the disk radius at which fragmentation sets in. The McKee & Tan (2003) core collapse model is examined in more detail in §3: we compute angular momentum scales in §3.2 using formulae derived in the Appendix. In §4 we calculate expected fragmentation radii for a range of masses in the core collapse model.

Turning to the consequences of fragmentation, we examine in §5 the likely properties of stars born within fragments and the possibility that fragmentation limits accretion. In §5.2 we compare our results with observed regions of HMSF.

## 2 DISK FRAGMENTATION

### 2.1 Criterion for Fragmentation

We shall concentrate on fragmentation due to local gravitational instabilities, which set in when Toomre’s parameter

$$Q = \frac{c_{\text{ad}}\Omega}{\pi G\Sigma} \quad (1)$$

descends toward unity. Here  $\Sigma$  is the disk’s surface density,  $\Omega$  its orbital frequency, and  $c_{\text{ad}}$  is its adiabatic sound speed. (We shall frequently refer to the isothermal sound speed  $c_s = \gamma^{-1/2}c_{\text{ad}}$  where  $\gamma$  is the ratio of specific heats.)

Observational inferences of massive circumstellar tori (Cesaroni 2005) indicate that they may be subject to *global* instabilities as well. We discuss this possibility briefly in §4.4; however the local instabilities tend to occur first, and their relation to fragmentation is better understood.

Several authors have identified the fragmentation boundary in terms of a cooling time. Following Gammie (2001) and ML05, we convert this criterion to a critical mass accretion rate at a given midplane temperature. The cooling time  $\tau_c$  is the ratio of the internal energy per area,  $U = c_{\text{ad}}^2 \Sigma / [\gamma(\gamma - 1)]$ , to the dissipation rate per unit area – which, in steady accretion, is

$$2F_v = \frac{3\dot{M}\Omega^2}{4\pi} \quad (2)$$

where  $F_v$  is the flux through each disk face. Eliminating  $\Sigma$ , the maximum accretion rate is

$$\dot{M}_{\text{max}} = \frac{4\gamma^{1/2}}{3(\gamma - 1)} \frac{c_s^3}{Q\Omega\tau_c G}. \quad (3)$$

For later convenience we write this in terms of the isothermal sound speed  $c_s = \gamma^{-1/2} c_{\text{ad}}$ . Extrapolating from Gammie (2001)'s two-dimensional simulations for a stiff equation of state, ML05 estimate  $\dot{M}_{\text{max}} = 0.89c_s^3/G$  for the case of a three-dimensional,  $\gamma = 5/3$  disk. Using smoothed-particle hydrodynamics, Rice et al. (2005) have simulated just such a disk, finding  $\Omega\tau_c$  to lie between 6 and 7 when it fragments. Assuming also  $Q = 1$ , this implies  $\dot{M}_{\text{max}} = (0.37 \text{ to } 0.43)c_s^3/G$ . For a fixed  $\dot{M}$ , the critical temperature is then significantly (1.6 times) higher than ML05 estimated.

At face value this weakens the conclusion, reached by ML05, that fragmentation is unattainable in low-mass protostellar disks. However, more recent simulations show that disks remain stable at shorter  $\tau_c$  depending on how abruptly cooling is implemented (E. Harper-Clark 2006, private communication). Due to uncertainties in the aforementioned cooling factor, and in light of the stringent resolution requirements for collapse outlined by Nelson (2006), we consider the value of  $\Omega\tau_c$  obtained by Rice et al. (2005) to be uncertain by up to a factor of two. We shall therefore be conservative, by adopting the stricter ML05 criterion that fragmentation occurs when

$$c_s < c_{s,\text{crit}} = 1.04(G\dot{M}_{\star d})^{1/3}. \quad (4)$$

Since the mass accretion rate is comparable to  $\varepsilon c_{\text{eff}}(\text{core})^3/G$  in the core collapse scenario, where  $c_{\text{eff}}(\text{core})^2$  is the ratio of pressure to density in the core, equation (4) implies, qualitatively, that a disk fragments if its sound speeds falls below the effective sound speed of its parent core (see equation [23] below). This point was made for thermally supported cores by ML05, and equation (4) simply extends the rule to turbulent cores.

Equation (4) is conservative in the sense that fragmentation may also occur at somewhat higher values of  $c_s$ . It is even more conservative given that  $\gamma$  declines from 5/3 at the higher temperatures relevant to massive star formation. We shall make several other conservative estimates in order to show that disk instability is all but inevitable during massive star formation.

When assessing disk stability in a given scenario, we first calculate the midplane temperature profile  $c_s(r)$  of the disk given its central mass  $M_{\star}$ , central luminos-

Subscript	Meaning
cl ...	Clump
c....	Core
★....	Star
d....	Disk
★d....	Star-disk system
f....	Final value
crit..	Critical value for fragmentation
irr...	Stellar irradiation
v....	Viscous flux

ity  $L_{\star}$ , and accretion rate  $\dot{M}_{\star d}$ . For this we adopt the Shakura & Sunyaev  $\alpha$  parametrization of viscosity, in which the steady mass accretion rate is

$$\dot{M}_{\text{visc}} = \frac{3\pi\alpha\Sigma c_s^2}{\Omega}. \quad (5)$$

For the choice of critical temperature made in equation (4) this corresponds to  $\alpha = 0.30Q$  at the onset of fragmentation. We keep  $\alpha$  fixed at 0.30 throughout our analysis, as this correctly reproduces the fragmentation boundary, although this is an overestimate for stable disks.

Having identified the *fragmentation radius* as the location where the disk sound speed falls to the critical value in equation (4), we then compare this to the characteristic disk radius

$$R_d = \frac{j^2}{GM_{\star}} \quad (6)$$

for accreting gas with specific angular momentum  $j$ .

We set the viscous accretion rate equal to the accretion rate from the envelope, and let  $Q = 1$ . We then check whether the disk can remain in this steady state with two models for heat generation. In §2.2 we ignore the luminosity from the protostar and find a minimum value for  $T_d(r)$  using only the viscous generation of heat. Next, in §2.3, we include the flux from the protostar received at the disk surface, and again solve for the midplane temperature as a function of radius.

## 2.2 Viscous Heating

In a thermal steady state, the flux of viscous energy radiated by each face of the disk is given by equation (2). All of the disks considered in this paper are optically thick to their own thermal radiation; therefore, the flux can also be derived from radiation transfer across an optical depth  $\kappa\Sigma/2$  from the disk midplane to its surface:

$$F_r = \frac{8}{3\tau_R} \sigma T_d^4, \quad (7)$$

where  $\tau_R = \kappa_R \Sigma_d / 2$  is the optical depth corresponding to the Rosseland mean opacity  $\kappa_R(T_d)$ . The factor 8/3 in equation (7) is derived by assuming that the dissipation rate per unit mass is a constant (Chick & Cassen 1997). We obtain temperature dependent opacities from Semenov et al. (2003). These opacities are very insensitive to density; we adopt values for  $10^{-12.5} \text{ g cm}^{-3}$ , an appropriate value for a disk with  $Q = 1$  and a period of a few centuries.

Neglecting irradiation of the disk surface, in a steady state  $F_v = F_r$  and  $\dot{M}_{\text{visc}} = \dot{M}_{\star d}$ . We solve for  $\Sigma$  in equation

(5), and then  $c_s$  from equations (2) and (7) using  $\mu c_s^2 = k_B T$  (for molecular weight  $\mu$ ), yielding

$$c_s^{10} = \frac{3k_B^4 \kappa_R \dot{M}_{*d}^2 \Omega^3}{128\pi^2 \sigma \mu^4 \alpha}. \quad (8)$$

This is an implicit formula for  $c_s$ , as  $\kappa_R$  depends on temperature. Equating  $c_s$  to  $c_{s,\text{crit}}$  (equation 4) implies fragmentation when

$$\Omega < 8.54 \left( \frac{\sigma \mu^4 \alpha G^{10/3} \dot{M}_{*d}^{4/3}}{k_B^4 \kappa_R} \right)^{1/3}. \quad (9)$$

In practice we calculate the run of  $c_s(r)$  and  $\kappa_R(r)$  self-consistently in order to evaluate equation (9).

Whereas ML05 found a unique value of  $\Omega_{\text{crit}}$  for optically thick accretion disks around low-mass protostars, we shall show below that equation (9) gives a roughly constant fragmentation radius of about 130 AU. The key difference is the higher accretion rate, which implies much higher critical temperature (hundreds of K) in massive star formation compared to  $\sim 16$  K for the low mass case. As the opacity law does not obey  $\kappa_R(T) \propto T^2$  for these higher temperatures, the ML05 result does not hold for these more massive stars.

### 2.3 Stellar Irradiation

Stars of mass somewhat greater than  $10M_\odot$  undergo Kelvin-Helmholtz contraction rapidly enough to settle onto the hydrogen burning main sequence while still accreting. As the main sequence luminosity increases rapidly with  $M_*$ , the consequences of stellar luminosity become acute for massive stars. One such consequence is the heating of the disk midplane due to reprocessed stellar radiation. In principle, this stabilizes disks to longer periods (larger radii) than we found in equation (9) by considering only viscous heating. We parametrize irradiation through the reprocessing factor  $f$  defined as the ratio between the incident flux  $F_{\text{irr}}$  normal to the disk surface, and the spherical stellar flux at that radius:

$$F_{\text{irr}} = \frac{fL}{4\pi R_d^2}. \quad (10)$$

A calculation of  $f$  requires a model for the reprocessing of starlight onto the disk.

#### 2.3.1 Infall geometry

ML05 model  $f$  in the context of an infall geometry similar to that used by Whitney & Hartmann (1993) and Kenyon et al. (1993) for scattered-light images of protostars. Starlight is absorbed at the inner edge of a rotating infall envelope (Chevalier 1983; Terebey et al. 1984) whose innermost streamlines have been removed by the ram pressure of a magnetically collimated protostellar wind. This removal implies a suppression of the star-disk accretion rate relative to the rate at which mass would otherwise accrete – from the surrounding core, for instance, in a core-accretion model:

$$\dot{M}_{*d} = \varepsilon \dot{M}_c; \quad (11)$$

where  $\varepsilon = \cos \theta_0$  if streamlines are removed from all angles within  $\theta_0$  of the axis. (We assume the prestellar matter is isotropically distributed before it falls in.)

The balance of forces that determines  $\varepsilon$  is modeled in detail by Matzner & McKee (2000) for low-mass star formation, and we expect that their analysis holds into the massive star regime. The location of the innermost streamline is a simple function of  $\varepsilon$ : it strikes the disk at a radius

$$(1 - \varepsilon^2)R_d. \quad (12)$$

The calculation of  $f$  is particularly simple if the dust envelope is (1) optically thick to stellar photons; (2) optically thin to dust thermal radiation; and (3) not hot enough to sublimate. Under these conditions, ML05 find

$$f \simeq 0.1\varepsilon^{-0.35} \quad (13)$$

for a reasonable range of  $\varepsilon$ .

#### 2.3.2 Envelope self-opacity and dust sublimation

It is important to examine the assumptions that led to equation (13), especially in the context of very rapid accretion onto very massive stars.

In §3.2 we will estimate the typical infall column density  $\Sigma_{\text{sph},f}$  in a core collapse scenario, and find it to be a few times lower than the core column  $\Sigma_c$ , i.e.,  $\Sigma_{\text{sph},f} \simeq 0.3 \text{ g cm}^{-2}$ . Given that the Semenov et al. (2003) Planck opacity peaks between 3 and  $16 \text{ cm}^2 \text{ g}^{-1}$  for  $45 < T < 930$  K, we expect the disk midplane to be shielded by moderate optical depths ( $\sim 1-5$ ) from the reprocessing surface. A solution to the radiation diffusion problem is beyond the scope of this paper. Instead we will apply equation (13); this is conservative, in the sense that it overestimates the stabilizing effect of irradiation.

A further potential complication arises for especially high accretion rates, those in excess of  $1.7 \times 10^{-3} M_\odot \text{ yr}^{-1}$ . The critical temperature of such a disk is quite hot,  $T_{\text{crit}} > 1050$  K according to equation (4). As we shall see in §4, the stabilizing effect of irradiation is accentuated in these disks by a sharp drop in Rosseland opacity. If the disk is to reach 1050 K, however, dust in the nearby infall envelope must approach the silicate sublimation temperature of about 1500 K. This leads to the disappearance of dust within the infall envelope inside a certain *sublimation radius*  $R_s$ . Monnier & Millan-Gabet (2002) determine  $R_s \simeq 35(L_*/10^6 L_\odot)^{1/2}$  AU by optical interferometry (and note that this value requires the existence of large silicate grains). We expect that disks with  $R_d > R_s$  are relatively unaffected by dust sublimation. We do not attempt to calculate disk irradiation in cases where this is not true.

#### 2.3.3 Incorporation into fragmentation calculation

Solving equation (10), we can find the equilibrium temperature of the outer reaches of an optically thick disk for which irradiation dominates over viscous heating. While low-mass protostellar disks can be stabilized in this regime (ML05), massive-star disks are not. We therefore account self-consistently for  $T_d(R_d)$ , in two steps. The disk's effective (surface) temperature ( $T_s$ , say) is determined by the requirement that it emit the viscous flux in addition to re-emitting the incident flux:

$$\sigma T_s^4 = F_v + F_{\text{irr}}. \quad (14)$$

The midplane temperature  $T_d$  is derived from  $T_s$  from radiation diffusion of the viscous flux across optical depth  $\tau_R$ ,

$$\begin{aligned} \sigma T_d(R_d)^4 &= \sigma T_s^4 + \frac{8}{3} \tau_R F_v = \left( \frac{8}{3} \tau_R + 1 \right) F_v + F_{\text{irr}} \\ &\simeq \frac{8}{3} \tau_R F_v + F_{\text{irr}}. \end{aligned} \quad (15)$$

We account for the temperature dependence of the opacity when solving this equation numerically.

As before, we identify the critical disk radius  $R_{\text{crit}}$  at which  $T_d(R_d) = T_{\text{crit}}$ . Fragmentation occurs if the disk extends beyond  $R_{\text{crit}}$ .

### 2.3.4 Other Considerations

We pause to address two minor concerns:

*Shock Heating*– Infalling matter is decelerated in an accretion shock upon reaching the disk, and heat radiated by this shock warms the disk surface. However the gravitational potential at  $R_d$  is very small compared to that at the stellar surface, as  $R_d \gg R_*$ . Moreover, the star’s emission is dominated by hydrogen burning rather than accretion, and a fair fraction of the starlight is reradiated onto the disk surface in our model (eq. 13). Shock heating is thus wholly negligible (by about four orders of magnitude, for a  $30 M_\odot$  star).

*Radiation Pressure*– When  $Q = 1$  the ratio of gas to radiation pressure at a characteristic fragmentation radius is

$$\frac{P_g}{P_{\text{rad}}} = \frac{3k_B \Omega^2}{2\pi G a \mu T_{\text{crit}}^3} = 10^{1.8} \frac{30 M_\odot}{M_*} \left( \frac{t_{\text{acc}}}{10^5 \text{ yr}} \right)^2 \left( \frac{150 \text{ AU}}{R_d} \right)^3, \quad (16)$$

where  $t_{\text{acc}}$  is the duration of accretion (see §§2.4 and 3.1). Radiation pressure remains negligible out to periods of 3300 years (scaling as  $(M_* \Sigma)^{-3/4}$  in the core model of §3). Moreover the photon diffusion time across the scale height  $H$ ,  $t_{\text{diff}} \simeq 3\tau_R H/c$ , is a few hundred times shorter than the orbital period. Consequently photon pressure is irrelevant for disk fragmentation during massive star formation.

## 2.4 Typical Parameters for Fragmentation

Before treating the core accretion model in detail in §3, we wish to draw a few conclusions that are reasonably independent of a scenario for massive star formation. We adopt in our irradiation model a fiducial efficiency parameter  $\varepsilon = 0.5$ , but we consider other values in §4.2.

We begin by mapping the maximum disk radius and maximum disk angular momentum as functions of the stellar mass  $M_*$  and the accretion time,  $t_{\text{acc}} = 2M_*/\dot{M}_{*d}$ . (The factor of two derives from the core accretion scenario of McKee & Tan 2003; accretion time is simply a convenient parametrization for accretion rate.) The results for  $R_{\text{crit}}$  and  $j_{\text{crit}}$  are shown as the solid curves in figures 1 and 2, respectively.

Not all of this parameter space is relevant, however. Observations of protostellar outflows emerging from sites of massive star formation imply dynamical ages of order  $10^5$  years. On both of these figures, we highlight within the dotted lines a plausible range of  $t_{\text{acc}}$  as the range of values predicted by McKee & Tan (2003) for core column densities ( $\Sigma_c$ ) of  $0.3 - 3 \text{ g cm}^{-2}$ . One may further restrict one’s attention to masses between 10 and  $120 M_\odot$ , as more massive

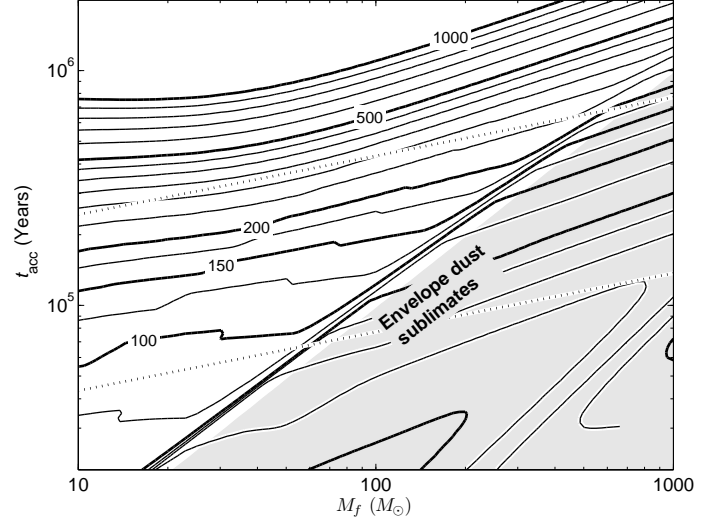


**Figure 1.** The fragmentation radius (in AU) is shown for a range of central star masses and accretion times. Also shown is the star formation time in the core model (dotted lines, for  $0.3 < \Sigma_{\text{cl}} < 3 \text{ g cm}^{-2}$ ) and the region affected by dust sublimation in the infall envelope (filled region), where our model does not hold. The sharp kink in the lines of constant radius is due to a drop in opacity for disk temperatures above about 1050K.

# in fig. 3	$\log_{10} j \text{ (cm}^2 \text{ s}^{-1}\text{)}$	Reference
1	22.3	Cesaroni et al. (2005)
2	21.4	Patel et al. (2005)
5	22.1	Zhang et al. (2002)
6	22.0	Bernard et al. (1999)
9	21.6	De Buizer & Minier (2005)

**Table 1.** Estimates of angular momentum of observed disks in figure 3 and corresponding references. Angular momentum estimates are computed from the observed velocity gradient over the extent of the disk. Estimates are only made for data points that showed a clear velocity gradient associated with a disk or torus.

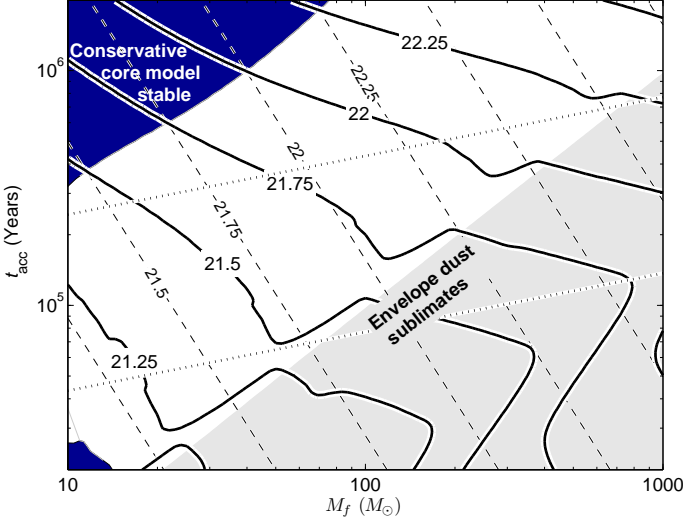
stars are not known to exist. From this we infer: *for plausible values of the accretion time scale, massive-star accretion disks fragment for radii above about 100-200 AU, with 150 AU being a typical threshold.*

Table (1) lists our estimates for the angular momentum of several observed disks, most of which appear likely to fragment.

## 3 CORE ACCRETION

With these relatively model-independent results in hand, let us evaluate disk fragmentation in the turbulent core model (Myers & Fuller 1992; McKee & Tan 2003), which posits that massive stars accrete from hydrostatic structures (cores, subscript “c”) that have assembled from an overdense region (clump, subscript “cl”) within a larger molecular cloud. This is similar to the standard model of low-mass star formation, except that turbulent motions are subsonic within low-mass cores (e.g., ML05) and supersonic in massive cores.

To calculate core and core collapse properties, we adopt



**Figure 2.** Angular momentum and disk fragmentation. The critical value of angular momentum, labeled as  $\log_{10}(j_{\text{crit}})$ , is plotted as *bold curves* for a range of stellar masses and formation times,  $t_{\text{acc}} = 2M_{\star}/(M_{\star,d})$ . *Dashed lines* show our predicted angular momentum for the McKee & Tan (2003) core model ( $\varepsilon = 0.5$ ,  $k_{\rho} = 1.5$ ). As discussed in §3.2, this is also an approximate upper limit to  $j$  given  $M_{\star}$  and  $t_{\text{acc}}$ . Disks tend to fragment except in the upper, dark filled region. In the lower, light filled region, envelope dust grains sublimate within  $R_d$ ; our model is not secure here. *Dotted lines* delimit core model formation times for  $0.3 < \Sigma_{\text{cl}} < 3 \text{ g cm}^{-2}$ .

the McKee & Tan (2003) models and fiducial parameters. Turbulent cores are modeled as singular polytropic spheres with density profiles  $\rho(r) \propto r^{-k_{\rho}}$ , with  $k_{\rho} \simeq 1.5$ . Since they are assumed to be hydrostatic (see also Tan et al. 2006), they must be pressure confined within their parent clumps. McKee & Tan 2003 evaluate the mean hydrostatic pressure within clumps to be

$$\bar{P}_{\text{cl}} = 0.88G\Sigma_{\text{cl}}^2 \quad (17)$$

Further, they assume that massive cores are segregated to the centers of clumps where the pressure is roughly twice  $\bar{P}_{\text{cl}}$ . Fixing cores' surface pressure to this value implies, for fiducial parameters, that  $\Sigma_c = 1.22\Sigma_{\text{cl}}$ . Observations imply a column density  $\Sigma_{\text{cl}}$  of around  $1 \text{ g cm}^{-2}$  for the clumps that host massive star formation (Plume et al. 1997; Hillenbrand & Hartmann 1998; Figer et al. 1999; Kim et al. 2000; van den Bergh et al. 1991; Gilbert & Graham 2001; de Marchi et al. 1997; Turner et al. 2000; Faúndez et al. 2004).

As cores are bound and argued not to fragment (Krumholz 2006), their gas either accretes on the star (a fraction  $\varepsilon$ ) or is blown out by the protostellar wind ( $1 - \varepsilon$ ). The final stellar mass is therefore  $M_{\star,f} = \varepsilon M_c$ , with  $\varepsilon \simeq 0.5$ , and the core radius is

$$R_c = \frac{0.040}{\varepsilon^{1/2}\Sigma_{\text{cl,cgs}}^{1/2}} \left( \frac{M_{\star,f}}{30M_{\odot}} \right)^{1/2} \text{ pc} \quad (18)$$

where  $\Sigma_{\text{cl,cgs}}$  is in  $\text{g cm}^{-2}$ .

In the following sections we shall refer to  $\sigma = \sigma(r)$ , the local velocity dispersion of core gas at radius  $r$ ; in a singular polytropic core,

$$\sigma(r)^2 = \frac{4\pi}{6\phi_B(k_{\rho} - 1)} \frac{GM_c(r)}{r} \quad (19)$$

where  $M_c(r)$  is the enclosed mass, and  $\phi_B \equiv P/(\rho\sigma^2)$  accounts for magnetic contributions to the total pressure; McKee & Tan (2003) estimate  $\phi_B \simeq 2.8$ .

We note, in passing, that the fiducial core model implicitly assumes that stellar accretion halts due to a limited mass supply, rather than due to the onset of vigorous stellar feedback, fragmentation of the core or disk, or any other dynamical effect. Alternatively one could either have  $\varepsilon = M_{\star,f}/M_c \ll 1$ , or one could define the core to be the sub-region that successfully accretes (for which  $\varepsilon \sim 0.5$ ). In the latter choice, the pressure-equilibrium column,  $\sim 1.22\Sigma_{\text{cl}}$ , would provide only a lower limit to  $\Sigma_c$ . As it is widely held that the upper mass cutoff derives from stellar feedback, we expect columns in excess of this lower limit to prevail for very massive stars. Nevertheless, we evaluate the above equations for  $\Sigma_c = 1.22 \text{ g cm}^{-2}$  in the fiducial case.

### 3.1 Collapse

McKee & Tan (2003) show that the accretion time is close to the free-fall time evaluated at the core's surface density. Their equations (3), (4), (5), (35), and (36) specify

$$\dot{M}_{\star,d} = \varepsilon\phi_{\text{acc}} \frac{\sigma^3}{G} \quad (20)$$

where

$$\begin{aligned} \phi_{\text{acc}} &= 0.71(3.38 - k_{\rho})(k_{\rho} - 1)^{3/2}(3 - k_{\rho})^{1/2} \\ &\times \begin{cases} \frac{\phi_B^{3/2}}{(1+H_0)^{1/2}}, & \text{magnetic} \\ 1, & \text{nonmag.} \end{cases} \\ &\rightarrow 1.9 \end{aligned} \quad (21)$$

where the magnetic term includes levitation by the static field (the factor  $(1 + H_0) \simeq 2$ ) as well as turbulent magnetic pressure (the factor  $\phi_B$ ). The second line evaluates the first for a magnetized core with  $k_{\rho} = 1.5$ , for which the final accretion time is

$$t_{\text{acc}} = 1.3 \times 10^5 \Sigma_{\text{cl,cgs}}^{-3/4} \left( \frac{0.5 M_{\star,f}}{\varepsilon 30M_{\odot}} \right)^{1/4} \text{ yr} \quad (22)$$

(McKee & Tan 2003). Equation (21) implies fragmentation when

$$c_s < 1.04(\varepsilon\phi_{\text{acc}})^{1/3}\sigma, \quad (23)$$

i.e., for  $c_s < 1.02\sigma$  when  $\varepsilon = 0.5$  and  $\phi_{\text{acc}} = 1.9$ .

During collapse, distribution of mass,  $M_c(r) \propto r^{3-k_{\rho}}$ , and free-fall time,  $t_{\text{ff}}(r) \propto \rho(r)^{-1/2}$ , imply

$$\begin{aligned} M_{\star} &= (t/t_{\star,f})^{\eta_m} M_{\star,f} \quad \text{and} \\ \dot{M}_{\star,d} &= \frac{\eta_m M_{\star}}{t} \propto M_{\star}^{1-1/\eta_m} \quad \text{where} \\ \eta_m &= \frac{6}{k_{\rho}} - 2 \rightarrow 2. \end{aligned} \quad (24)$$

The accretion time is longer than the Kelvin-Helmholtz time for stars  $\gtrsim 10M_{\odot}$  (Wolfire & Cassinelli 1987), implying that massive protostars reach the zero age main-sequence (ZAMS) during accretion. When calculating the time evolution of fragmentation in §4.3, we employ the McKee & Tan

(2003) models for the luminosity of a massive accreting protostar; to calculate irradiation at the end of accretion we also include ZAMS luminosity, using formulae from Tout et al. (1996).

### 3.2 Angular Momentum

To evaluate our fragmentation criterion, we require the angular momentum of material within a collapsing turbulent core. Although this is not included in the McKee & Tan (2003) models, we shall estimate angular momentum within these models by generalizing a calculation by ML05 (itself an analytical version of the Burkert & Bodenheimer 2000 calculation, in the vein of Fleck 1987). This calculation (presented in the Appendix) notes that a core model specifies the turbulent velocity dispersion  $\sigma(r)$  as well as the density profile  $\rho(r)$ . For a special class of velocity fields one can compute the ensemble-averaged specific angular momentum and velocity dispersion. The velocity field must be isotropic; it must have a velocity difference between any two points that scales as  $\sigma(|\mathbf{r}_1 - \mathbf{r}_2|) \propto |\mathbf{r}_1 - \mathbf{r}_2|^\beta$  regardless of the underlying density distribution; and its Cartesian components must be uncorrelated (i.e., transport no average shear stress). The ensemble-averaged specific angular momentum and velocity dispersion are calculated in equations (44)-(47). We define the *spin parameter*  $\theta_j$  for a turbulent region of size  $R$ :

$$\theta_j \equiv \frac{j}{R\sigma(R)} = f_j \frac{\langle j^2 \rangle^{1/2}}{R \langle \sigma(R)^2 \rangle^{1/2}}. \quad (25)$$

The rightmost expression involves root-mean-square ensemble averages over the turbulent velocity field, which are calculated in the Appendix. The factor  $f_j$  accounts for the difference between the ratio of rms averages and the ratio of amplitudes; since the amplitudes are random variables, this includes both an overall offset and a dispersion. ML05 estimate  $\log_{10} f_j = -0.088_{-0.49}^{+0.16}$  on the basis of a Gaussian model for the velocity field.

Our evaluation of the spin parameter is presented in the Appendix and summarized in figure 7 and table 7. For a turbulence supported region with  $\rho \propto r^{-k_\rho}$  one must have  $\sigma(r)^2 \propto GM(r)/r \propto r^{2-k_\rho}$ , so  $\beta = 1 - k_\rho/2 \rightarrow 1/4$  (for  $k_\rho \rightarrow 3/2$ ). In the McKee & Tan core collapse model, each shell of matter accretes in sequence. For each shell, the spin parameter is

$$\theta_j(\text{shell}) = 0.85\beta^{0.42} f_j \rightarrow 0.47f_j \quad (26)$$

(see equation 49). However, the last shell to accrete naturally has the highest angular momentum; as the disk accumulates vector angular momentum, it may overestimate the disk radius. Moreover, although collapse is generally super-Alfvénic, magnetic braking may sap  $j$  somewhat. A rough lower bound on  $\theta_j$  is given by the specific angular momentum of the entire core, which corresponds to

$$\theta_j(\text{entire core}) = 0.50\beta^{0.55} f_j \rightarrow 0.23f_j \quad (27)$$

(also equation 49).

Given upper and lower limits for  $\theta_j$ , we must decide which value to adopt. The remainder of this paper is intended to establish that fragmentation is inevitable in the outer reaches of massive-star disks, so we shall adopt the more conservative estimate (eq. 27). Please bear in mind

that the upper bound to  $R_d$  is about four times larger. The protostellar outflow will tend to remove low- $j$  material (see also ML05), but we expect this effect to be rather minor and do not evaluate it.

For convenience we shall define a second rotation-related quantity,  $\phi_j$ , by

$$j = \frac{\phi_j GM_\star}{\varepsilon \sigma}. \quad (28)$$

The factor  $\phi_j$  defined here is related to the spin parameter  $\theta_j$  by  $\phi_j = R\sigma(R)^2\theta_j/[GM(R)]$ . Hydrostatic equilibrium requires  $R\sigma(R)^2/[GM(R)] = 1/[2(k_\rho - 1)\phi_B]$ : therefore

$$\phi_j = \frac{\theta_j}{2(k_\rho - 1)\phi_B} \rightarrow 0.36\theta_j \quad (29)$$

giving  $\phi_j = 0.067$  in the fiducial case.

The disk acquires a final radius which is about 1/40th of the core radius:

$$\begin{aligned} R_{d,f} &= \frac{\theta_j \phi_j}{\varepsilon} R_c \\ &\rightarrow 300 \left(\frac{0.5}{\varepsilon}\right)^{3/2} \left(\frac{M_{\star f}}{30 M_\odot} \frac{1}{\Sigma_{\text{cl, cgs}}}\right)^{1/2} \text{AU} \end{aligned} \quad (30)$$

in the fiducial, conservative case given by equation (27). During accretion, the disk radius remains proportional to the current radius of accretion; therefore

$$\frac{R_d}{R_{d,f}} = \left(\frac{M_\star}{M_{\star f}}\right)^{\frac{1}{3-k_\rho} \rightarrow 2/3}, \quad (31)$$

at least on average.

It is useful to know the column density scale in the infall for reference in the calculation of disk irradiation. As discussed in ML05, this is characterized by  $\Sigma_{\text{sph}}(R_d)$ : the column outward from  $R_d$  in a nonrotating infall of the same accretion rate. We find

$$\begin{aligned} \Sigma_{\text{sph}}(R_{d,f}) &= \frac{\epsilon \phi_{\text{acc}}}{2^{5/2}(k_\rho - 1)\phi_B \theta_j} \Sigma_c \\ &\rightarrow 0.64 \Sigma_c \end{aligned} \quad (32)$$

i.e., that the final infall column is comparable to the core column (see also ML05). Over the course of accretion,

$$\frac{\Sigma_{\text{sph}}(R_d)}{\Sigma_{\text{sph}}(R_{d,f})} = \left(\frac{M_\star}{M_{\star f}}\right)^{\frac{1-k_\rho}{3-k_\rho} \rightarrow -1/3}. \quad (33)$$

Finally, a note on the relation between a core's density profile and its angular momentum scale. Considering the range of values  $1 \leq k_\rho \leq 2$ , the angular momentum of a turbulent sphere decreases sharply toward zero as  $k_\rho$  approaches 2 and  $\beta$  approaches zero, as shown in figure 7. This trend is easily understood: when  $\beta = 0$ , the velocity difference between two points is independent of their separation and must therefore be contained in very small-scale motions as in an isothermal gas. Indeed, the three-dimensional power spectrum scales as  $k^{-3-2\beta}$  and contains a divergent energy at small scales as  $\beta \rightarrow 0$ . Angular momentum is dominated by the largest-scale motions that fit within the region of interest, and therefore vanishes if turbulent energy appears only at small scales. However, a core whose hydrostatic support is effectively isothermal ( $\beta = 0$ ) may still contain angular momentum due to *background* turbulence if it is confined in a turbulent region with  $\beta > 0$ . This situation holds

for thermally supported cores within turbulent molecular clouds, and formed the basis for the ML05 estimate of disk radii in low-mass star formation.

Background turbulence may increase  $j$  for turbulent cores, as well, if the density profile flattens and the effective value of  $\beta$  increases across the core boundary. Our calculation in the Appendix assumes that velocity field is described by the same  $\beta$  everywhere, so the corrected value of  $\theta_j$  should be intermediate between the core's  $\beta$  and that of the parent clump.

### 3.3 Observations of Rotation in HMSF

Goodman et al. (1993) observe velocity gradients of dense cores, including both low and high-mass cores, using  $\text{C}^{18}\text{O}$ ,  $\text{NH}_3$  and  $\text{CS}$  as tracers. They find that the ratio of rotational to gravitational energy, which we call  $\beta_{\text{rot}}$  (to avoid confusion with  $\sigma \propto r^\beta$ ), takes a rather broad distribution around a typical value of 0.02, i.e.,  $\log_{10} \beta_{\text{rot}} = -1.7$ . In our model for rotation within singular polytropic cores,

$$\beta_{\text{rot}} = \frac{(5 - 2k_\rho)^2}{8(3 - k_\rho)(k_\rho - 1)} \frac{\theta_j^2}{\phi_B}. \quad (34)$$

Using  $\theta_j = 0.23f_j$  as we estimated for the entire core (eq. [27]) this gives  $\log_{10} \beta_{\text{rot}} \simeq -2.1 \pm 0.7$ , whereas using  $\theta_j = 0.47f_j$  as appropriate to the outer shell (eq. [26]),  $\log_{10} \beta_{\text{rot}} \simeq -1.7 \pm 0.7$ . The agreement would thus be good if the Goodman et al. observations traced the outermost core gas, but this seems unlikely. A better explanation is that the observed cores have somewhat flatter density profiles; the discrepancy is removed if  $k_\rho = 1.35$  rather than 1.5 (using eqs. [42] and [49]). As noted above, embedding the core within a clump medium that has a flatter density profile (and higher  $\beta$ ) would have the same effect. Protostellar outflows also raise  $j$  slightly by removing material on axis. Of course, our model for core angular momentum is based on an idealized turbulent velocity spectrum, and undoubtedly involves some error.

We include observations of disks and toroids in massive star forming regions in figure (3) and table 2. However it should be noted that such comparisons are limited due to uncertainty in both the values of quoted parameters and in the actual phenomena being observed. Only recently has it been possible to achieve the resolution and sensitivity required to constrain models of massive star formation. Many uncertainties remain when distinguishing between infall, rotation (Keplerian or otherwise), and outflow. Many of the objects show velocity gradients that are consistent with Keplerian rotation, but could also be attributed to another bulk motion, such as infall. Furthermore even when rotation is indeed Keplerian, it is difficult to distinguish the disk edge from its natal core (De Buizer & Minier 2005; Cesaroni 2005; De Buizer 2006). This, and confusion with the outflow (De Buizer 2006), may cause disk masses and extents to be overestimated. The mass, luminosity and multiplicity of the central object involve further uncertainties.

We have already noted that the angular momentum seen in observations coincides with our estimated upper bound from the core collapse model. Although we think this agreement is likely to be real, it is also possible that the observed rotation is about a stellar group rather than a single object. This alternative is strengthened by the fact

that many rotating envelopes are inferred to be more massive than any single central object, on the basis of the central luminosity. Such overweight disks are subject to strong *global* self-gravitational instabilities quite distinct from the local instability we addressed in §2. We refer the reader to Shu et al. (1990) on this point; see also the discussion in §4.4 and that given in ML05.

It is notable that the three observations most confidently interpreted as thin massive-star disks (Patel et al. 2005; De Buizer & Minier 2005; Shepherd et al. 2001) are the best match to our predictions. The other, more extended massive disks or toroids are of uncertain mass and radius and may enclose many stars. As noted by Cesaroni (2005) and Beuther et al. (2006), in these instances we might be seeing proto-cluster, rather than protostellar, disks and toroids.

## 4 FRAGMENTATION OF CORE-COLLAPSE DISKS

A numerical evaluation of fragmentation is presented below in §4.1, but first we calculate the scalings that govern these results. Given the fragmentation criterion from §2.1 and the fiducial core-collapse model described in §3, we can estimate the ratio  $T_d/T_{\text{crit}}$  by ignoring either irradiation (“active” disks, as in §2.2) or viscous heating (“passive” disks, using §2.3):

$$\frac{T_d(R_d)}{T_{\text{crit}}} = \begin{cases} 0.15 \left( \frac{\varepsilon_{0.5}^{7.7} \kappa_{R,\text{cgs}}^4 \Sigma_{\text{cgs}}^5}{M_{\star f,30}^7} \right)^{1/20}, & \text{(active disk)} \\ 0.35 \left( \frac{L_\star}{\varepsilon_{0.5}^{1/60} M_{\star f,30}^3 \Sigma_{\text{cgs}}^{1/4}} \right)^{1/4}, & \text{(passive disk)} \end{cases} \quad (35)$$

where  $L_\star = 10^5 L_5 L_\odot$ ,  $\varepsilon = 0.5\varepsilon_{0.5}$ ,  $\kappa_R = \kappa_{R,\text{cgs}} \text{cm}^2 \text{g}^{-1}$ , and  $\Sigma = \Sigma_{\text{cgs}} \text{g cm}^{-2}$ .

Note that increasing  $M_{\star f}$  destabilizes disks in both regimes. High values of  $\Sigma$  enhance viscous heating relative to irradiation, but neither is sufficient to prevent fragmentation around a  $30 M_\odot$  star when  $\Sigma \sim 1 \text{g cm}^{-2}$ . However, if we take  $L = 20$  and  $\Sigma = 0.034 \text{g cm}^{-2}$  – values typical of the low-mass star formation studied by ML05 – then  $T_d(R_d) > T_{\text{crit}}$  for  $M > 1.3 M_\odot$  according to equation (35). The evaluation used here neglects several effects treated in that paper, such as thermal core support. Nevertheless these scalings explain why disks are intrinsically less stable during massive star formation than in the low-mass case, as seen in detail below.

### 4.1 Results

Fragmentation is expected when  $R_{d,f} > R_{d,\text{crit}}$ , i.e., when the disk extends past the critical fragmentation radius at some point during formation. Figure 3 compares these two radii for a range of stellar masses, using the fiducial, conservative core collapse model ( $k_\rho = 3/2$ ,  $\varepsilon = 0.5$ ,  $\Sigma_{\text{cl}} = 1 \text{g cm}^{-2}$ ,  $\theta_j = 0.23f_j$ ) to compute  $R_d$ .

To address the lowest-mass stars whose disks can fragment, we must account for the thermal component of a core's hydrostatic pressure and for the accretion luminosity, both of which are negligible in very massive stars. We have (1) included a thermal component (at 20 K) in the effective temperature that sets the accretion rate, so that

$\dot{M}_{*d} \geq 10^{-5.3} \epsilon M_{\odot} \text{yr}^{-1}$  for all masses; (2) added accretion luminosity to the ZAMS luminosity when estimating disk irradiation; and (3) employed the Palla & Stahler (1992) models (for  $\dot{M}_{*d} = 10^{-4} M_{\odot} \text{yr}^{-1}$ , which is appropriate) to estimate the radius of the accreting protostar. Although rather approximate, these amendments are of diminishing importance as  $M_{*f}$  increases beyond  $\sim 20 M_{\odot}$ .

Given the expected range of disk radii, all the disks presented in figure 3 are candidates for fragmentation. The expected disk radius crosses the fragmentation boundary for  $M_{*f} \simeq 3.5 M_{\odot}$ , and the two remain almost equal until  $M_{*f} \simeq 10 M_{\odot}$ ; fragmentation is marginal in this range. Fragmentation becomes increasingly likely as the mass increases, though slowly:  $R_{\text{crit}}$  is within a factor of 2 of  $R_d$  for  $M_{*f} < 23 M_{\odot}$ . For  $M_{*f} > 57 M_{\odot}$ ,  $R_{\text{crit}}$  drops below the range of disk radii implied by the dispersion of  $f_j$  given below equation (25) – as indicated by the gray region in figure 3. The specific masses quoted depend on our model for angular momentum, particularly as the critical radius is relatively constant in the range 100-150 AU.

Recall, however, that the disk angular momentum derives from a turbulent velocity field and is therefore quite stochastic. The spread in  $j$  predicted by a Gaussian model for the velocity field allows for the frequent formation of disks twice as large as predicted in equation (30). Likewise, much smaller disks (by about a factor of nine) can form equally easily from a chance cancellation within the core velocity field. This dispersion in expected radii is indicated as a shaded band in figure 3. Remember also that we adopted a conservative estimate of the disk angular momentum; otherwise, disk fragmentation would have been even more prevalent. Taking these points into account, we can draw a few conclusions with relative certainty.

(i) A *significant portion* of the O star and early B star protostellar disks predicted in the core collapse model are prone to fragmentation, although the exact fraction is sensitive to the (uncertain) angular momentum scale and fragmentation criterion;

(ii) The tendency of disks to fragment increases with stellar mass ( $M_{*f}$ ); it decreases with higher column densities ( $\Sigma_{\text{cl}}$ ), and with steeper initial density profiles ( $k_{\rho}$ ).

(iii) Disks accreting more rapidly than about  $1.7 \times 10^{-3} M_{\odot} \text{yr}^{-1}$  are destabilized by the sharp drop in dust opacity at  $\sim 1050$  K, according to equation (4). In the fiducial core model, this occurs above about  $110 M_{\odot}$ , close to the observed upper limit of stellar masses. More generally, this occurs for  $M_{*f} > 87 (t_{\text{acc}}/10^3 \text{yr}) M_{\odot}$ .

(iv) At somewhat higher accretion rates, however, dust sublimation invalidates our model for starlight reprocessing in the infall envelope.

(v) So long as disks remain optically thick, any effect that decreases the Rosseland opacity is destabilizing. For instance, low-metallicity disks are less stable than those of solar composition. (Primordial disks are however opaque in their inner portions. Tan & McKee 2004) By adopting the (relatively opaque) Semenov et al. (2003) dust opacities, we have underestimated disk fragmentation.

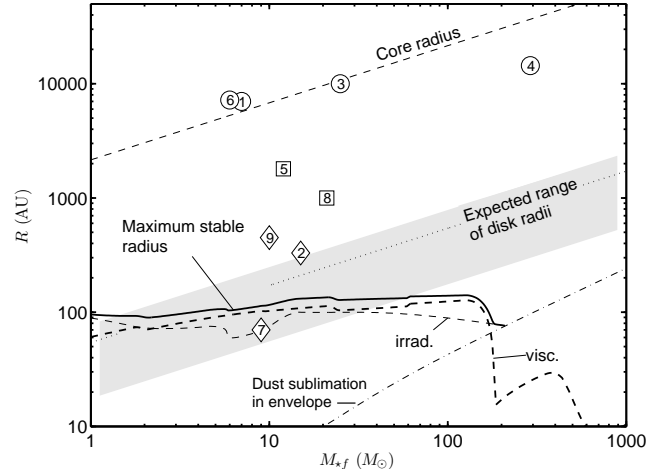


**Figure 3.** Relevant radii. The characteristic disk radius predicted by (fiducial) core accretion is accompanied by a shaded band illustrating our (Maxwellian) model for its dispersion. The largest stable radius is plotted for comparison; this is accompanied by the contributions from pure irradiation (no viscous heat) and pure viscosity (no irradiation). The turnover of  $R_{\text{crit}}$  above  $\sim 20 M_{\odot}$  is due to the scaling of ZAMS mass and luminosity. The references for the observational points are listed in table (2). Circles represent objects that may best be described as cores, whereas diamonds represent those objects whose disks are well resolved. Squares indicate objects for which it is unclear whether they are rotating, infalling, or both; see §5.2 for discussion.

Number in figure 3	Reference
1	Cesaroni et al. (2005)
2	Patel et al. (2005)
3	Olmi et al. (2003)
4	Olmi et al. (2003)
5	Zhang et al. (2002)
6	Bernard et al. (1999)
7	Shepherd et al. (2001)
8	Shepherd et al. (2001)
9	De Buizer & Minier (2005)

**Table 2.** Observational data points in figure 3 and corresponding references.

## 4.2 Effect of Varying Efficiency

Up to this point we have adopted  $\epsilon = 0.5$  as the fiducial accretion efficiency, following McKee & Tan (2003). In the theory of Matzner & McKee (2000),  $\epsilon$  is set by the ejection of material by a centrally-collimated protostellar wind. Matzner & McKee show that  $\epsilon$  is quite insensitive to the ratio of infall and outflow momentum fluxes. Nevertheless, 0.5 is only an estimate and  $\epsilon$  could well vary during accretion. This is especially true if the protostellar wind were ever to truncate accretion, as  $\epsilon(t) \rightarrow 0$  when this happens. We briefly consider other values here.

The primary effect of varying  $\epsilon$ , while fixing  $M_{*f}$ ,  $\Sigma_{\text{cl}}$ , and  $k_{\rho}$ , is to change the core mass required to make a star of that mass. Suppose we halve  $\epsilon$ , so that  $M_c$  must double. The accretion time then increases, and  $\dot{M}_{*d}$  decreases, by a factor  $2^{1/4}$  (for  $k_{\rho} = 3/2$ ). This mildly stabilizes the disk. But at the same time,  $R_c$  has been increased by  $2^{1/2}$ ,  $j$  has gone



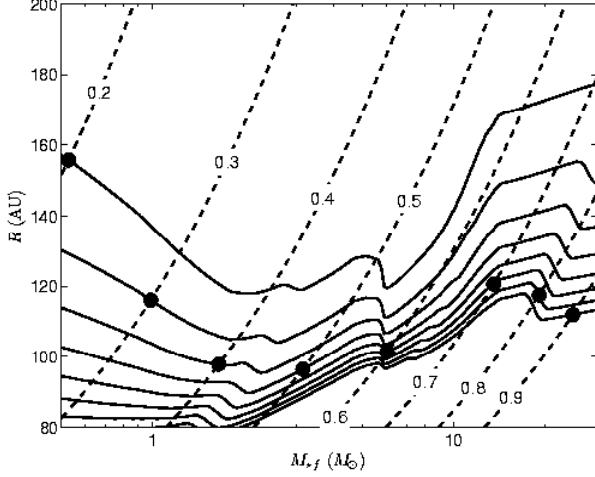


**Figure 4.** Effect of varying the star formation efficiency  $\varepsilon$  in the fiducial core collapse model. *Dashed lines*: critical disk radius  $R_{d,\text{crit}}$  for fragmentation; *solid lines*: expected disk extent  $R_d$ . Intersections are as marked.

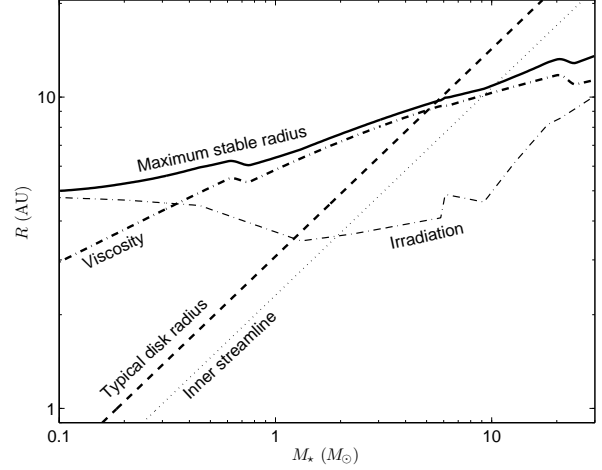
up by  $2^{3/4}$ , and  $R_{d,f}$  has expanded by  $2^{3/2}$ . Balancing these contributions, we expect lowering  $\varepsilon$  to destabilize the disk. This was predicted also in equation (35), where lowering  $\varepsilon$  is seen to decrease stability in an active disk. Passive disks are extremely insensitive to  $\varepsilon$ .

Figure (4) corroborates our expectation by showing that lower values of  $\varepsilon$  correspond to less stable disks. Indeed, the mass at which fragmentation sets in is sensitive to  $\varepsilon$ , specifically,  $M_{\text{crit}} \propto \varepsilon^{2.6}$ , while the critical disk radius is relatively constant. Does this mean that a decline in core efficiency over time destabilizes disks? Probably not, since most of the mass will be accreted at an intermediate value of  $\varepsilon$  (see the discussion below equation 18).

### 4.3 Time Evolution of Disk Fragmentation

For those disks that do suffer fragmentation, it is useful to know whether this happens early or late in accretion and how much matter is potentially affected. To address these questions we construct the time history of the accretion rate, stellar mass, and disk radius for a star with  $M_{*f} = 30 M_{\odot}$  in the fiducial core collapse model. For this calculation we use the luminosity history of such a star as presented by McKee & Tan (2003). The scalings  $R_d(t) \propto M_*(t)^{1/(3-k_\rho)}$  and  $\dot{M}_d(t) \propto M_*(t)^{(6-2k_\rho)/(6-3k_\rho)}$  permit us to gauge disk fragmentation through time.

Figure (5) shows the evolution of  $R_d$  and  $R_{\text{crit}}$  during accretion. In this plot, the relative constancy of the fragmentation radius is due to the enhanced effect of irradiation at low masses. We find that a star destined to become  $30 M_{\odot}$  (born of a  $60 M_{\odot}$  core) has a disk that crosses into the regime of fragmentation when the protostar has accreted approximately  $5.6 M_{\odot}$ . The fact that this is slightly higher than the critical mass identified earlier is to be expected: the inner  $5.6 M_{\odot}$  of a larger core is equivalent to a  $5.6 M_{\odot}$  core with a slightly higher column density – specifically,  $\Sigma_c \propto (M_*/M_{*f})^{-1/3}$ , for  $k_\rho = 3/2$  (cf. equation 33). The somewhat higher column density implies a smaller and



**Figure 5.** Growth of disk and critical radius with the mass of a protostar accreting toward  $30 M_{\odot}$  in the fiducial core collapse model. In addition to the expected disk radius, we show the splashdown radius of the inner infall streamline, calculated assuming  $\varepsilon = 0.5$ .

somewhat stabler disk, leading to a slightly higher mass scale for fragmentation.

We also show on figure (5) the radius of the innermost streamline of infalling material from the envelope from Terebey et al. (1984), again assuming an accretion efficiency of 50%. This, along with stochastic variations in disk angular momentum about its typical value, suggest that accretion can coexist with fragmentation so long as the disk is not too far beyond the fragmentation threshold; see §5.3 for more discussion.

### 4.4 Disk mass and global instability

At the typical fragmentation radius of 100 – 150 AU, the mass scale of a disk with  $Q = 1$  is

$$\frac{\pi R_d^2 \Sigma_d(R_d)}{M_{*f}} = 0.10 \varepsilon_{0.5}^{1/12} \left( \frac{R_d}{150 \text{ AU}} \right)^{1/2} \frac{\Sigma_{\text{cgs}}^{1/4}}{M_{*f,30}^{1/4}}. \quad (36)$$

Global instabilities of the disk are triggered by the total disk mass (Adams et al. 1989; Shu et al. 1990), which is larger than  $\pi R_d^2 \Sigma_d(R_d)$  by the factor  $2/(2 - k_\Sigma)$  if  $\Sigma_d \propto r^{-k_\Sigma}$  within  $R_d$ . There is therefore the possibility that the fast angular momentum transport by these modes (Laughlin et al. 1998) suppresses local fragmentation, but we consider it unlikely that fragmentation is eliminated by this process.

## 5 CONSEQUENCES OF INSTABILITY

### 5.1 Fragment Masses

Once a disk fragments, what objects form? Goodman & Tan (2004) determine the *initial* fragment mass based on the wavenumber of the most unstable mode in the disk. The corresponding wavelength of this axisymmetric mode is:

$$\lambda(r) = 2\pi \frac{c_{\text{ad}}^2}{\pi G \Sigma}, \quad (37)$$

where  $\Sigma$  and  $c_s$  are both functions of radius within the disk. Assuming that the fragment has comparable dimension azimuthally, the corresponding mass scale is (Goodman & Tan 2004)

$$\begin{aligned} M_{\text{frag}} &= \lambda^2 \Sigma \\ &= \frac{4\pi c_{\text{ad}}^3}{\Omega G} Q, \end{aligned} \quad (38)$$

i.e., roughly the amount of mass accreted in  $2Q$  orbits. We assume fragmentation only occurs when  $Q \rightarrow 1$ . We consider our rather idealized estimate of  $M_{\text{frag}}$  uncertain by at least a factor of two. In reality the initial mass is likely a stochastic variable, best determined from numerical simulations (R. Rafikov, private communication).

Once a fragment forms, its growth is controlled by accretion of surrounding gas, migration through the disk, and collisional or gravitational interaction with other fragments. Rather than address these questions in detail, we will draw preliminary conclusions by comparing  $M_{\text{frag}}$  to two critical scales: the gap opening mass  $M_{\text{gap}}$  and the isolation mass  $M_{\text{iso}}$ . A fundamental uncertainty is the state of the gas disk: again, we assume  $Q = 1$ .

When the gravitational torques exerted on the disk by the fragment exceed viscous torques, a gap opens around the fragment. Rafikov (2002) estimates

$$\begin{aligned} M_{\text{gap}} &= \frac{2c_{\text{ad}}^3 \alpha}{3\Omega G 0.043} \\ &= 0.37 \frac{\alpha/0.30}{Q} M_{\text{frag}}. \end{aligned} \quad (39)$$

Since this is less than  $M_{\text{frag}}$ , and gets even smaller if the disk viscosity goes down and thus cooling time goes up relative to the critical state in the Gammie (2001) simulations, we expect fragments to open gaps immediately.

Gap opening slows but does not necessarily end accretion (Artymowicz & Lubow 1996). A possible limit to growth is set by the point at which the fragment accretes all the mass within its Hill radius (e.g., Goodman & Tan 2004, but see Artymowicz & Lubow). This defines the isolation mass

$$M_{\text{iso}}(r) \approx \frac{(2\pi f_H r^2 \Sigma)^{3/2}}{9M_\star^{1/2}} \quad (40)$$

where  $f_H \simeq 3.5$ .

Figure (6) compares the initial, gap opening, and isolation masses for a range of  $M_\star$ , evaluated at  $R_{\text{crit}}$  near the end of core accretion (in the fiducial core model). Because gap opening slows accretion, we expect the masses of disk-born stars to resemble  $M_{\text{frag}}$  more than  $M_{\text{iso}}$ . In this case they will be low-mass stars of order 0.2–0.4  $M_\odot$ .

Fragmentation tends to set in at  $\sim 100 - 200$  AU, as we noted in §2.4. However gap-opening fragments should be swept inward if disk accretion continues; only a single disk mass of accretion is required to bring them in to the central object. If they move inward by about a factor of 30, they will be within a few stellar radii at carbon ignition (Webbink 1985). As candidates for mass transfer and common-envelope evolution, such objects can serve as reservoirs of matter and angular momentum for the relic of the central star's supernova explosion.

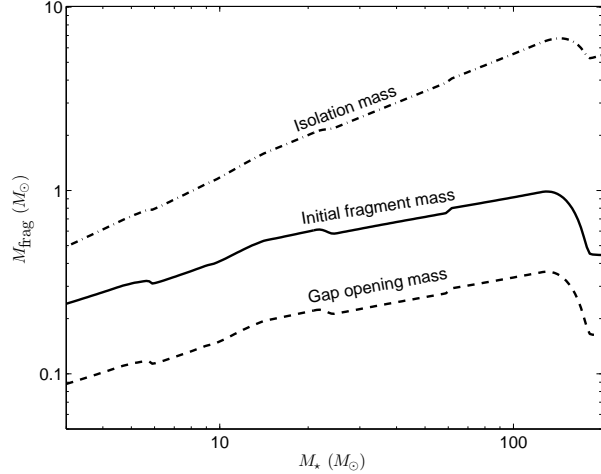


**Figure 6.** Our estimate of the initial fragment mass, compared to the gap opening mass and isolation mass, at the end of accretion in the fiducial core collapse model. We truncate the calculation where dust sublimation in the envelope makes the critical radius determination uncertain.

## 5.2 Observability of Disk-Born Stars

We have predicted that stars with extended protostellar disks will produce low mass (M5–G5) companions. Thus we would expect many O stars, and perhaps some early B stars, to have multiple coplanar companions at separations of order  $\lesssim 100 - 200$  AU, depending on the amount of migration that occurs following formation. In the closest clusters, for example, Orion, this corresponds to an angular separation of approximately  $0.4''$  and an apparent bolometric magnitude difference of, at a minimum,  $\sim 13$  magnitudes. This implies that even in K-band with an AO system such as that of VLT, such objects would be difficult to observe (M. Ahmic, private communication). Similarly, the combination of AO with a coronagraph (e.g. the Lyot coronagraph on AEOS) can provide a dynamic range of up to up to 8 H-band magnitudes at a few hundred mas, which is still too small to detect the aforementioned companions (Hinkley et al. 2006). If not detectable during the main sequence life of the primary star, the presence of such companions might be observable via binary interaction once the primary evolves.

## 5.3 Disk Efficiency

If a  $30M_\odot$  star will suffer disk fragmentation early in its accretion, as we estimated in §4.3 on the basis of the turbulent core model, then we must address how this might impact subsequent accretion. One possibility is that gap-opening fragments will be swept inward to the central star, in which case its final mass will be unaffected. This outcome resembles the scenario outlined by Levin (2003) for gravitationally unstable AGN accretion. Alternatively, Tan & Blackman (2005) suggest low-luminosity AGN may be starved of gas by fragmentation.

In the latter scenario, a strongly unstable disk will have a low *disk efficiency*,  $\varepsilon_d \equiv \dot{M}_\star / \dot{M}_{\star d}$ . We can estimate  $\varepsilon_d$  in the limit that none of the gas entering an unstable region of the disk ultimately accretes onto the star. The splash-down radius of the innermost streamline was estimated in

expression (12). Given that outflow removes matter from the inner streamlines, and that fragmentation removes it from the outer portions of the disk, the fraction of mass that successfully accretes (after striking the disk) is

$$\varepsilon_d = 1 - \varepsilon^{-1} \left[ 1 - \left( 1 - \frac{R_{\text{crit}}}{R_d} \right)^{1/2} \right]. \quad (41)$$

Of course, this expression is only applicable when it yields  $0 \leq \varepsilon_d \leq 1$ , i.e., when the disk is partly but not wholly unstable.

Two complications arise when evaluating equation (41). First, the critical radius  $R_{\text{crit}}$  must be calculated using the mass accretion rate outside of itself. Second, recall that the angular momentum of infalling gas derives from its initial turbulent velocity and is likely to vary in direction and magnitude. The fluctuations of  $j$  were estimated by the distribution  $f_j$ , which appeared in equation (25). Accounting for both of these effects, we find that accretion can continue even in an actively unstable disk. For  $30M_\odot$ , we find that the infall streamline remains within the stable disk radius through the end of accretion. Even if all the gas entering a fragmenting region is consumed, this need not fully starve the central object. However, the tendency to fragment becomes much stronger for more massive stars. This is especially true for those ( $M_{*f} \sim 110M_\odot$ , from §4) that accrete rapidly enough that their disks are destabilized by the drop in dust opacity.

In reality, we expect some gas to accrete through the unstable region. A rough upper limit would be to adopt the accretion rate for a Toomre-critical ( $Q = 1$ ) state, and assume that any surplus is consumed by fragmentation. In this case, the central accretion rate would be limited by the temperature of the coldest region of the disk (according to eq. 4). Numerical simulations will ultimately be required to quantify the behaviour of Toomre-unstable disks.

Furthermore, there are numerous feedback mechanisms that have not been addressed. For example, if fragmentation halts accretion, this could change the outflow power, the shape of the outflow and infall cavity and thus the heating of the disk by reprocessed starlight. This interplay will be investigated in future work.

## 6 DISCUSSION

Our primary conclusion (§2.4) is that massive-protostar disks that accrete more slowly than  $\sim 1.7 \times 10^{-3} M_\odot \text{ yr}^{-1}$  are subject to fragmentation at disk radii beyond about 150 AU. This critical radius is set primarily by the viscous heating of the disk midplane as it accretes, with reprocessed starlight playing an equal or secondary role for most stellar masses. As all the disks we consider are optically thick, the critical radius depends on the Rosseland opacity law  $\kappa_R(T)$  within dusty disk gas.

Comparing to our conservative estimate of the disk radius in the McKee & Tan (2003) model for massive star formation by the collapse of turbulent cores (§3), we find that fragmentation is marginal for stars accreting four to 15 solar masses; higher-mass stars are increasingly afflicted by disk fragmentation. Although the mass at which fragmentation sets in is sensitive to our somewhat uncertain fragmentation criterion (§2.1) and angular momentum calculation

(§3.2 and the Appendix), we have been conservative in five ways: (1) by adopting a fragmentation temperature lower than that implied by the Rice et al. (2005) simulations; (2) by adopting a low estimate of the specific angular momentum that determines the disk radius; (3) by adopting a relatively opaque model for the disk's Rosseland opacity; (4) by ignoring the shielding effect of a moderately opaque infall envelope, and (5) by adopting a low estimate for the cooling time, and a hard equation of state. All of these approximations should, if anything, lead us to underestimate the prevalence of disk fragmentation. Along with the existence of turbulent fluctuations in  $j$  (§4), these points ensure that *some* massive stars above  $\sim 10M_\odot$  experience disk fragmentation. As noted in §4.4, we cannot rule out the possibility that global instabilities flush disk material fast enough to suppress fragmentation, but we consider it unlikely that this prevents *all* fragmentation.

We therefore expect multiple, coplanar, low-mass (M5 to G5, §5.1) companions to form around many O (and some B) stars. Given initial separations of order 100-200 AU, their photospheric emission is not observable with present techniques. Disk migration, followed by mass transfer or common-envelope evolution, may however make them evident as the primary evolves (§5.2).

Even when disks fragment, we expect some accretion onto the central star – if only because of material that falls within the fragmentation radius (§5.3). Although we cannot yet quantify the disk efficiency parameter  $\varepsilon_d$ , we expect it to be significantly less than unity for those early O stars ( $M_{*f} \gtrsim 50M_\odot$ ) whose disks are most prone to fragment.

### 6.1 Imprint on the initial mass function

The stabilizing effect of viscous heating is absent in disks that accrete more rapidly than  $1.7 \times 10^{-3} M_\odot \text{ yr}^{-1}$ , thanks to a sharp drop in dust opacity at  $\sim 1050$  K (see §4). As this affects stars of mass greater than  $87(t_{\text{acc}}/10^5 \text{ yr})M_\odot$ , or about  $110 M_\odot$  in the fiducial core model, it may be related to the cutoff of the initial mass function (IMF) at about  $120 M_\odot$ .

Several other explanations for this cutoff have been proposed, all involving the increasing bolometric luminosity, ionizing luminosity, or outflow force emitted by the central star. Starvation by disk fragmentation has the distinctive feature that it becomes much more severe at a specific accretion rate. For this reason we expect it to produce a sharper IMF cutoff. (The transition to super-Eddington luminosities could also produce a sharp cutoff, but Krumholz et al. 2005 argue that this can be overcome by asymmetric radiation transfer.)

Note also that disk accretion is *destabilized* by rapid accretion, whereas rapid accretion quenches the effects of direct photon force and of the ionizing radiation (Wolfire & Cassinelli 1987). Disk fragmentation may close an avenue by which very massive stars would otherwise form.

### 6.2 Proto-binary disks

Pinsonneault & Stanek (2006) state that close massive binaries ( $< 10$  year periods) are more likely to have nearly equal masses. More generally, the binarity fraction overall

among massive stars is higher than their low mass counterparts (1.5 versus 0.5, Bally et al. (2005)). Due to the high fraction of roughly equal mass binaries, their effect on disk dynamics must be addressed in future work. Moreover, the stellar densities in regions of HMSF are high, suggesting that other cluster stars might be close enough to interfere with disks stretching out to  $\sim 100$  AU (Bate et al. 2003). It is not currently clear whether disk accretion can preferentially grow a low-mass companion until its mass rivals that of the primary star, as Artymowicz & Lubow (1996) suggest. If so, then disk fragmentation may be relevant in the production of equal-mass binaries; if not, they must form by another mechanism. In any case, the multiplicity of the center of gravity should be accounted for in future work. It seems unlikely, though, that a binary with  $\sim 10$  year period will stabilize the fragmenting regions whose periods are  $\gtrsim 300$  years.

**Acknowledgments:** We are pleased to thank the referee, Jonathan Tan, for very useful suggestions, as well as Ray Jayawardhana, Scott Kenyon, Chris McKee, Stefan Mochnecki, Roman Rafikov, Debra Shepherd, and Yanqin Wu for helpful discussions, and Alyssa Goodman for a leading question. We would also like to thank Susana Lizano for insightful suggestions regarding disk observations. C.D.M.'s research is funded by NSERC and the Canada Research Chairs program. K.M.K. is supported by a U. Toronto fellowship.

## REFERENCES

- Adams F. C., Ruden S. P., Shu F. H., 1989, *ApJ*, 347, 959  
 Artymowicz P., Lubow S. H., 1996, *ApJ*, 467, L77+  
 Bally J., Cunningham N., Moeckel N., Smith N., 2005, in Cesaroni R., Felli M., Churchwell E., Walmsley M., eds, IAU Symp. 227, *Nearby regions of massive star formation*. Cambridge Univ. Press, Cambridge, p.12. pp 12–22  
 Bate M. R., Bonnell I. A., Bromm V., 2003, *MNRAS*, 339, 577  
 Bernard J. P., Dobashi K., Momose M., 1999, *A&A*, 350, 197  
 Beuther H., Churchwell E. B., McKee C. F., Tan J. C., 2006, *ArXiv Astrophysics e-print* 2012  
 Burkert A., Bodenheimer P., 2000, *ApJ*, 543, 822  
 Cesaroni R., 2005, *Ap&SS*, 295, 5  
 Cesaroni R., Neri R., Olmi L., Testi L., Walmsley C. M., Hofner P., 2005, *A&A*, 434, 1039  
 Chevalier R. A., 1983, *ApJ*, 268, 753  
 Chick K. M., Cassen P., 1997, *ApJ*, 477, 398  
 Chini R., Hoffmeister V., Kimeswenger S., Nielbock M., Nürnberger D., Schmidtobreich L., Sterzik M., 2004, *Nature*, 429, 155  
 De Buizer J. M., 2006, *ApJ*, 642, L57  
 De Buizer J. M., Minier V., 2005, *ApJ*, 628, L151  
 de Marchi G., Clampin M., Greggio L., Leitherer C., Nota A., Tosi M., 1997, *ApJ*, 479, L27+  
 Faúndez S., Bronfman L., Garay G., Chini R., Nyman L.-Å., May J., 2004, *A&A*, 426, 97  
 Figer D. F., Kim S. S., Morris M., Serabyn E., Rich R. M., McLean I. S., 1999, *ApJ*, 525, 750  
 Fleck Jr. R. C., 1987, *ApJ*, 315, 259  
 Gammie C. F., 2001, *ApJ*, 553, 174  
 Gilbert A. M., Graham J. R., 2001, *Bulletin of the American Astronomical Society*, 33, 1330  
 Goodman A. A., Benson P. J., Fuller G. A., Myers P. C., 1993, *ApJ*, 406, 528  
 Goodman J., Tan J. C., 2004, *ApJ*, 608, 108  
 Hillenbrand L. A., Hartmann L. W., 1998, *ApJ*, 492, 540  
 Hinkley S. et al., 2006, *ArXiv Astrophysics e-print* 9337  
 Kenyon S. J., Whitney B. A., Gomez M., Hartmann L., 1993, *ApJ*, 414, 773  
 Kim S. S., Figer D. F., Lee H. M., Morris M., 2000, *ApJ*, 545, 301  
 Krumholz M. R., 2006, *ApJ*, 641, L45  
 Krumholz M. R., McKee C. F., Klein R. I., 2005, *ApJ*, 618, L33  
 Laughlin G., Korchagin V., Adams F. C., 1998, *ApJ*, 504, 945  
 Levin Y., 2003, *ArXiv Astrophysics e-print* 7048  
 Matzner C. D., Levin Y., 2005, *ApJ*, 628, 817  
 Matzner C. D., McKee C. F., 2000, *ApJ*, 545, 364  
 McKee C. F., Tan J. C., 2003, *ApJ*, 585, 850  
 Monnier J. D., Millan-Gabet R., 2002, *ApJ*, 579, 694  
 Myers P. C., Fuller G. A., 1992, *ApJ*, 396, 631  
 Nelson A. F., 2006, *ArXiv Astrophysics e-print* 9493  
 Olmi L., Cesaroni R., Hofner P., Kurtz S., Churchwell E., Walmsley C. M., 2003, *A&A*, 407, 225  
 Palla F., Stahler S. W., 1992, *ApJ*, 392, 667  
 Patel N. A., Curiel S., Sridharan T. K., Zhang Q., Hunter T. R., Ho P. T. P., Torrelles J. M., Moran J. M., Gómez J. F., Anglada G., 2005, *Nature*, 437, 109  
 Pinsonneault M. H., Stanek K. Z., 2006, *ApJ*, 639, L67  
 Plume R., Jaffe D. T., Evans N. J. I., Martin-Pintado J., Gomez-Gonzalez J., 1997, *ApJ*, 476, 730  
 Rafikov R. R., 2002, *ApJ*, 572, 566  
 Rice, W. K. M., Lodato, G., & Armitage, P. J. 2005, *MNRAS*, 364, L56  
 Semenov D., Henning T., Helling C., Ilgner M., Sedlmayr E., 2003, *A&A*, 410, 611  
 Shakura N. I., Sunyaev R. A., 1973, *A&A*, 24, 337  
 Shepherd D. S., Claussen M. J., Kurtz S. E., 2001, *Science*, 292, 1513  
 Shu F. H., Tremaine S., Adams F. C., Ruden S. P., 1990, *ApJ*, 358, 495  
 Tan J. C., Blackman E. G., 2005, *MNRAS*, 362, 983  
 Tan J. C., Krumholz M. R., McKee C. F., 2006, *ApJ*, 641, L121  
 Tan J. C., McKee C. F., 2004, *ApJ*, 603, 383  
 Terebey S., Shu F. H., Cassen P., 1984, *ApJ*, 286, 529  
 Tout C. A., Pols O. R., Eggleton P. P., Han Z., 1996, *MNRAS*, 281, 257  
 Turner J. L., Beck S. C., Ho P. T. P., 2000, *ApJ*, 532, L109  
 van den Bergh S., Morbey C., Pazder J., 1991, *ApJ*, 375, 594  
 Webbink R. F., 1985, in Pringle J. E., Wade R. A., eds, *Interacting Binary Stars*. Cambridge Univ. Press, Cambridge, p. 39  
 Whitney B. A., Hartmann L., 1993, *ApJ*, 402, 605  
 Wolfire M. G., Cassinelli J. P., 1987, *ApJ*, 319, 850  
 Zhang Q., Hunter T. R., Sridharan T. K., Ho P. T. P., 2002, *ApJ*, 566, 982

Profile	$\beta = 1/4$	$\beta = 1/2$
turbulent core	0.2704	0.4206
critical Bonnor-Ebert sphere	0.2730	0.3828
uniform region ( $k_\rho = 0$ )	0.3430	0.4714
thin shell	0.4714	0.6324

**Table 3.** Values of  $\langle j^2 \rangle^{1/2} / (R \langle \sigma^2 \rangle^{1/2})$  in our model for turbulent angular momentum.

## 7 APPENDIX

We present here an estimate of the angular momentum of cores initially supported by turbulent motions, generalizing the results of ML05 to arbitrary line width-size relations. The analytical treatment of this problem rests on several idealizations about turbulent velocities: (1) that they are isotropic and homogeneous; and (2) that the Cartesian velocity components are neither correlated with each other, nor (to any appreciable degree) with density fluctuations. For simplicity we also assume (3) that the core density profile is spherically symmetric and can be captured in a single function  $\rho(r)$ . When evaluating our formulae we assume (4) that the velocity difference between two points scales as a power of their separation, and (5), for the purpose of computing fluctuations, that the velocity components are Gaussian random fields.

One might object that condition (1) is inconsistent with the turbulent support of an inhomogeneous density profile. Consider, however, that if the core profile is a power law  $\rho(r) \propto r^{-k_\rho}$ , then the turbulent line width must scale as  $\sigma(r) \propto r^\beta$  where

$$\beta = 1 - k_\rho/2. \quad (42)$$

A velocity field with this scaling is consistent with our conditions (1), (2), and (4) if

$$\langle [\mathbf{v}_i(\mathbf{r}_1) - \mathbf{v}_j(\mathbf{r}_2)]^2 \rangle = k |\mathbf{r}_1 - \mathbf{r}_2|^{2\beta} \delta_{ij} \quad (43)$$

where angle brackets represent an ensemble average and  $k$  is a normalization constant related to the virial parameter  $\alpha$ . ML05 considered the case  $\beta = 1/2$  appropriate for giant molecular clouds ( $k_\rho = 1$ ); we generalize their formulae to other values of  $\beta$ , including the fiducial value  $\beta = 1/4$  corresponding to  $k_\rho = 3/2$ .

Our goal is to compute the expectation value and dispersion of the core specific angular momentum  $j$ , normalized to  $R_c \sigma$  where  $\sigma$  is the one-dimensional line width of the core. We find that, under our assumptions,

$$\langle j^2 \rangle = - \int \int \frac{d^3 \mathbf{r}_1 \rho(r_1)}{M} \frac{d^3 \mathbf{r}_2 \rho(r_2)}{M} \mathbf{r}_1 \cdot \mathbf{r}_2 \langle [v_x(\mathbf{r}_1) - v_x(\mathbf{r}_2)]^2 \rangle \quad (44)$$

and that

$$\langle \sigma^2 \rangle = \frac{1}{2} \int \int \frac{d^3 \mathbf{r}_1 \rho(r_1)}{M} \frac{d^3 \mathbf{r}_2 \rho(r_2)}{M} \langle [v_x(\mathbf{r}_1) - v_x(\mathbf{r}_2)]^2 \rangle \quad (45)$$

where  $M = \int \rho d^3 \mathbf{r}$  and all integrals are restricted to the region of interest (typically the core interior). These equations, which we will prove below, agree with the formulae in ML05's Appendix but allow  $\langle [v_x(\mathbf{r}_1) - v_x(\mathbf{r}_2)]^2 \rangle$  to be an arbitrary function of  $|\mathbf{r}_1 - \mathbf{r}_2|$ . It is important to note that the two formulae are identical up to the factor  $-2\mathbf{r}_1 \cdot \mathbf{r}_2$  in the integrand. The negative sign in equation (44) ensures that  $\langle j^2 \rangle$  is positive, since  $\langle [v_x(\mathbf{r}_1) - v_x(\mathbf{r}_2)]^2 \rangle$  takes higher values when  $|\mathbf{r}_1 - \mathbf{r}_2|$  is large, hence when  $\mathbf{r}_1 \cdot \mathbf{r}_2$  is negative.

To evaluate equations (44) and (45) we make use of spherical symmetry and impose equation (43) for the velocity correlations. Defining  $\mu = \mathbf{r}_1 \cdot \mathbf{r}_2 / (r_1 r_2)$  as the cosine of the angle between  $\mathbf{r}_1$  and  $\mathbf{r}_2$ ,

$$\begin{aligned} \langle j^2 \rangle &= -k \int_0^R dr_1 4\pi r_1^2 \frac{\rho(r_1)}{M} \int_0^R dr_2 2\pi r_2^2 \frac{\rho(r_2)}{M} r_1 r_2 (r_1^2 + r_2^2)^\beta \int_{-1}^1 d\mu (1 - q\mu)^\beta \mu \\ &= \frac{2\pi^2 k}{M^2} \int_0^R dr_1 \int_0^R dr_2 (r_1^2 + r_2^2)^{2+\beta} r_1 r_2 \rho(r_1) \rho(r_2) \left[ \frac{(1+q)^{\beta+2} - (1-q)^{\beta+2}}{\beta+2} - \frac{(1+q)^{\beta+1} - (1-q)^{\beta+1}}{\beta+1} \right] \end{aligned} \quad (46)$$

and

$$\begin{aligned} \langle \sigma^2 \rangle &= \frac{1}{2} k \int_0^R dr_1 4\pi r_1^2 \frac{\rho(r_1)}{M} \int_0^R dr_2 2\pi r_2^2 \frac{\rho(r_2)}{M} (r_1^2 + r_2^2)^\beta \int_{-1}^1 d\mu (1 - q\mu)^\beta \\ &= \frac{2\pi^2 k}{M^2} \int_0^R dr_1 \int_0^R dr_2 (r_1^2 + r_2^2)^{1+\beta} r_1 r_2 \rho(r_1) \rho(r_2) \left[ \frac{(1+q)^{\beta+1} - (1-q)^{\beta+1}}{\beta+1} \right] \end{aligned} \quad (47)$$

where  $q = 2r_1 r_2 / (r_1^2 + r_2^2)$ , as in ML05. Table 7 and figure 7 provide values of  $\langle j^2 \rangle^{1/2} / (R \langle \sigma^2 \rangle^{1/2})$  for several density profiles, both for the internal spectrum given by equation (42), and for  $\beta = 1/2$ , which may better represent the background spectrum.

Figure 7 plots the ratio  $\langle j^2 \rangle^{1/2} / (R \langle \sigma^2 \rangle^{1/2})$  as given by equations (46) and (47) for a turbulent core profile, a critical Bonnor-Ebert sphere, and a thin shell. The results are very close to power laws in  $\beta$ :

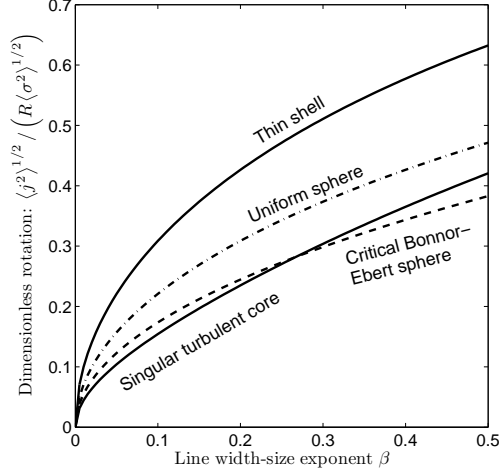


**Figure 7.** Values of  $\langle j^2 \rangle^{1/2} / (R \langle \sigma^2 \rangle^{1/2})$  evaluated for turbulence with line width-size exponent  $\beta$  and three relevant density profiles. For hydrostatic turbulent cores,  $\rho \propto r^{-2(1-\beta)}$ .

$$\frac{\langle j^2 \rangle^{1/2}}{R \langle \sigma^2 \rangle^{1/2}} \simeq \begin{cases} 0.655\beta^{0.638} & \text{singular turbulent core} \\ 0.537\beta^{0.488} & \text{critical Bonnor – Ebert sphere} \\ 0.648\beta^{0.459} & \text{uniform – density sphere} \\ 0.849\beta^{0.424} & \text{thin shell.} \end{cases} \quad (48)$$

The spin parameter  $\theta_j$  makes reference to the velocity dispersion  $\sigma(R)$  at radius  $R$ , rather than the mean velocity dispersion  $\langle \sigma^2 \rangle^{1/2}$  within  $R$ . For this we use the scaling  $\sigma^2 \propto GM/r \propto M^{2\beta/(3-k_\rho)}$  to derive

$$\frac{\sigma(R)^2}{\langle \sigma^2 \rangle} = 1 + \frac{2\beta}{3 - k_\rho}.$$

With this correction factor accounted for,  $\theta_j/f_j$  is still very close to a power law of  $\beta$ :

$$\frac{\theta_j}{f_j} \simeq \begin{cases} 0.504\beta^{0.552} & \text{singular turbulent core} \\ 0.987\beta^{0.651} & \text{uniform – density region} \\ 0.849\beta^{0.424} & \text{thin shell.} \end{cases} \quad (49)$$

(The last line is unchanged, as there is no correction for a thin shell.) These formulae were quoted in §3.2.

We now return to the derivation of equation (44); equation (45) is treated below. The  $z$  component of the specific angular momentum of the core is

$$\begin{aligned} j_z^2 &= \int d^3 \mathbf{r}_1 \int d^3 \mathbf{r}_2 \frac{\rho_1}{M} (x_1 v_{y1} - y_1 v_{x1}) \frac{\rho_2}{M} (x_2 v_{y2} - y_2 v_{x2}) \\ &= \frac{1}{M^2} \int d^3 \mathbf{r}_1 \int d^3 \mathbf{r}_2 \rho_1 \rho_2 (x_1 x_2 v_{y1} v_{y2} + y_1 y_2 v_{x1} v_{x2} - x_1 y_2 v_{y1} v_{x2} - y_1 x_2 v_{x1} v_{y2}); \end{aligned} \quad (50)$$

here, as below, we use subscripts 1 and 2 to indicate functions of  $\mathbf{r}_1$  and  $\mathbf{r}_2$ , i.e.,  $\rho_1 = \rho(\mathbf{r}_1)$ . On ensemble averaging of the second line, the last two terms in equation (50) become zero thanks to the  $\delta_{ij}$  in equation (43). The first two terms are equal, thanks to spherical symmetry; thus

$$\langle j_z^2 \rangle = \frac{2}{M^2} \int d^3 \mathbf{r}_1 \int d^3 \mathbf{r}_2 \rho_1 \rho_2 x_1 x_2 \langle v_{y1} v_{y2} \rangle. \quad (51)$$

Spherical symmetry allows us to replace  $x_1 x_2$  with  $\mathbf{r}_1 \cdot \mathbf{r}_2 / 3$  and  $j_z^2$  with  $j^2 / 3$ , so

$$\begin{aligned} \langle j^2 \rangle &= \frac{2}{M^2} \int d^3 \mathbf{r}_1 \int d^3 \mathbf{r}_2 \rho_1 \rho_2 \mathbf{r}_1 \cdot \mathbf{r}_2 \langle v_{y1} v_{y2} \rangle \\ &= \frac{1}{M^2} \int d^3 \mathbf{r}_1 \int d^3 \mathbf{r}_2 \rho_1 \rho_2 \mathbf{r}_1 \cdot \mathbf{r}_2 (\langle v_{y1}^2 \rangle + \langle v_{y2}^2 \rangle - \langle (v_{y1} - v_{y2})^2 \rangle). \end{aligned} \quad (52)$$

The first two terms within the brackets are zero, as spherical symmetry requires them to be even in the space coordinates while  $\mathbf{r}_1 \cdot \mathbf{r}_2$  is odd; the surviving term yields equation (44).

To prove equation (45) we write

$$M\sigma^2 = \int d^3 \mathbf{r} \rho(\mathbf{r}) (v_x - \bar{v}_x)^2 = \int d^3 \mathbf{r} \rho(\mathbf{r}) (v_x^2 - \bar{v}_x^2) \quad (53)$$

where  $\bar{\mathbf{v}} = \int \mathbf{v}\rho(\mathbf{r})/Md^3\mathbf{r}$  is the center of mass velocity. In equation (50) we replace  $\bar{v}_x^2$  with  $\int \int \mathbf{v}_1 \cdot \mathbf{v}_2 (\rho_1/M)(\rho_2/M)d^3\mathbf{r}_1d^3\mathbf{r}_2$ , and we bring the first term into similar form by multiplying it by  $\int (\rho_2/M)d^3\mathbf{r}_2 = 1$ :

$$\begin{aligned} M\sigma^2 &= \int d^3\mathbf{r}_1 \int d^3\mathbf{r}_2 \rho_1 \rho_2 v_{x1} (v_{x1} - v_{x2}) \\ &= \frac{1}{2} \int d^3\mathbf{r}_1 \int d^3\mathbf{r}_2 \rho_1 \rho_2 (v_{x1} - v_{x2})^2. \end{aligned} \tag{54}$$

The second line follows from the first by noting that the integral is antisymmetric under interchange of  $\mathbf{r}_1$  and  $\mathbf{r}_2$ . When averaged, it yields equation (45).